

# Universal non-monotonic structure in the saturation curves of MOT-loaded $\text{Na}^+$ ions stored in an ion-neutral hybrid trap: Prediction and observation

R. Blümel<sup>1</sup>, J. E. Wells<sup>2</sup>, D. S. Goodman<sup>2,3</sup>, J. M. Kwolek<sup>2</sup>, and W. W. Smith<sup>2</sup>

<sup>1</sup>*Department of Physics, Wesleyan University,  
Middletown, Connecticut 06459, USA*

<sup>2</sup>*Department of Physics, University of Connecticut,  
Storrs, Connecticut 06269, USA and*

<sup>3</sup>*Department of Sciences, Wentworth Institute of Technology,  
Boston, Massachusetts 02115, USA*

(Dated: December 7, 2024)

## Abstract

We predict that the steady-state ion number  $N_s$  for radio-frequency (rf) traps, loaded at a rate of  $\lambda$  particles per unit time, shows universal non-monotonic behavior as a function of loading rate  $\lambda$ . The shape of  $N_s(\lambda)$ , characterized by four dynamical regions, is universal in the sense that it is predicted to manifest itself in all rf traps independently of the details of their construction. For  $\lambda \ll 1$  particles / rf cycle (Region I), as expected,  $N_s(\lambda)$  increases monotonically with  $\lambda$ . However, contrary to intuition, at intermediate  $\lambda \sim 1$  particles / rf cycle (Region II),  $N_s(\lambda)$  reaches a maximum, followed by a minimum of  $N_s(\lambda)$  (Region III). For  $\lambda \gg 1$  particles / rf cycle (Region IV),  $N_s(\lambda)$  again rises monotonically. In Region IV numerical simulations, analytical calculations, and experiments show  $N_s(\lambda) \sim \lambda^{2/3}$ . We confirm this prediction experimentally with MOT-loaded  $\text{Na}^+$  ions stored in a hybrid ion-neutral trap.

PACS numbers: 37.10.Ty, 52.27.Jt, 52.50.Qt

Radio-frequency (rf) traps [1] are important devices in widespread use for the long-time storage of charged particles. These traps come in a multitude of shapes and sizes [1–5] and their applications range from high-resolution spectroscopy [6] to atomic clocks [7] and quantum computing [8]. Independent of their construction, all these traps have one theme in common: They need to be loaded with charged particles. The loading frequently occurs via a laser beam [9] or an electron gun [10], creating charged particles at a rate  $\lambda$  inside of a well-defined region close to the center of the trap. The following question arises: For a given loading rate  $\lambda$ , what is the number of particles,  $N_s$ , in the saturated, steady state? While the absolute values of  $N_s$  depend on the trap’s physical size and the details of its construction, the qualitative shape of  $N_s(\lambda)$ , as a function of  $\lambda$ , does not. In fact, we found that the shape of  $N_s(\lambda)$  is universal and shows four clearly defined dynamical regions. In this paper we (a) predict the qualitative shape of the universal  $N_s(\lambda)$  curve, (b) uncover the underlying physical mechanisms, and (c) experimentally verify our predictions with the help of a MOT-loaded ion-neutral trap [11]. Knowledge of the steady-state ion number  $N_s$  in the trap is important for many different types of experiments. For example, collision-rate measurements [11, 12] use the steady-state ion cloud to measure the total collision rate, because it ensures constant density, size, and temperature conditions during the measurement. This is particularly helpful when working with optically dark, closed-shell ions such as  $\text{Rb}^+$  and  $\text{Na}^+$ , for which it is difficult to measure the dynamics of the cloud size.

We have discovered a non-monotonic structure of the steady-state ion number  $N_s(\lambda)$  as a function of loading rate  $\lambda$  in molecular-dynamics loading simulations of a three-dimensional (3D) Paul trap. In our simulations particles are created, one at a time, at times  $t_k$ ,  $k = 1, 2, \dots$ , with zero initial velocity. Corroborated by earlier SIMION calculations [13], this is a good approximation for ions loaded via photoionization from a MOT between 1 and 0.1 mK. Assuming that the creation times are uncorrelated, the time intervals  $\Delta t_k = t_{k+1} - t_k$  are Poissonian distributed with probability distribution  $P(\Delta t) = \lambda \exp(-\lambda \Delta t)$ . Concerning their spatial distribution, we assume that the particles are created at random positions with uniform distribution within a spherical volume of radius  $R$ , centered at the origin of the trap. The temporal and spatial distributions implemented in our molecular-dynamics simulations model the shot-noise type photoionization creation of ions from a cold cloud of particles stored in a magneto-optic trap (MOT) [11]. In the time interval between any two creation

events, i.e. for  $t_k < t < t_{k+1}$ , the particles in the trap are governed by the equations of motion of an ideal 3D Paul trap, which, in dimensionless variables, are given by [14]

$$\ddot{\vec{r}}_i + [a - 2q \sin(2t)] \begin{pmatrix} x_i \\ y_i \\ -2z_i \end{pmatrix} = \sum_{\substack{j=1 \\ j \neq i}}^{N_k} \frac{\vec{r}_i - \vec{r}_j}{|\vec{r}_i - \vec{r}_j|^3}, \quad (1)$$

where  $i = 1, \dots, N_k$  labels the  $N_k$  particles present in the trap during the time interval  $t_k < t < t_{k+1}$ ,  $\vec{r}_i = (x_i, y_i, z_i)$  is the position of the  $i$ th particle in the trap,  $a, q$  are the Paul-trap control parameters [1, 14], and  $t$  is the dimensionless time. When arriving at  $t_{k+1}$ , and before creating the next particle, we check whether one or more particles have left the trap. Qualitatively modeling the conditions inside an actual rf trap, all particles are eliminated from the trap whose positions at time  $t = t_{k+1}$  exceed a critical distance,  $R_c$ , from the center of the trap. Absorption at  $R_c$  models the fundamental fact that due to unavoidable physical structures, such as electrodes, or instabilities induced by higher-order rf multipoles [4], all experimental traps have a finite trapping volume and particles that venture too far from the center of the trap are lost. Following instantaneous deletion of all particles with  $|\vec{r}_i| > R_c$ , the next particle is loaded at  $t = t_{k+1}$ . This procedure is followed for all  $t_k$  until a pre-specified maximal simulation time is exceeded.

The result of a typical trap loading simulation is shown in Fig. 1. The red, fluctuating line in Fig. 1 shows the time evolution of the particle number  $N(t)$  in the trap for  $\lambda = 1$  as a function of  $t$  (in rf cycles) for  $q = 0.2$ ,  $a = q^2/2$ ,  $R = 3$ , and  $R_c = 15$ . A near linear rise of  $N(t)$  is followed by a sharp bend into a steady state in which  $N(t)$  fluctuates around  $N_s = \langle N(t) \rangle_t$ , the time average of  $N(t)$  in the steady-state.

For many applications (see, e.g., [11, 12]) it is necessary to know  $N_s(\lambda)$  for a given rf trap. Figure 2 shows  $N_s(\lambda)$  as a function of loading rate  $\lambda$  for the same Paul trap control parameters used to generate Fig. 1. The resulting curve in Fig. 2 clearly shows four distinct regimes, labeled I to IV. Region IV is the most straightforward to understand physically and we discuss it first. In Region IV, the loading rate is so high that a large space-charge density develops in the loading region. The resulting large electric field, directed radially outwards, accelerates the loaded particles outward toward  $R_c$  at which point the particles are lost from the trap. The acceleration due to the electric field of the space charge completely overwhelms the acceleration due to the trapping forces. As a consequence of this, the particles' dynamics

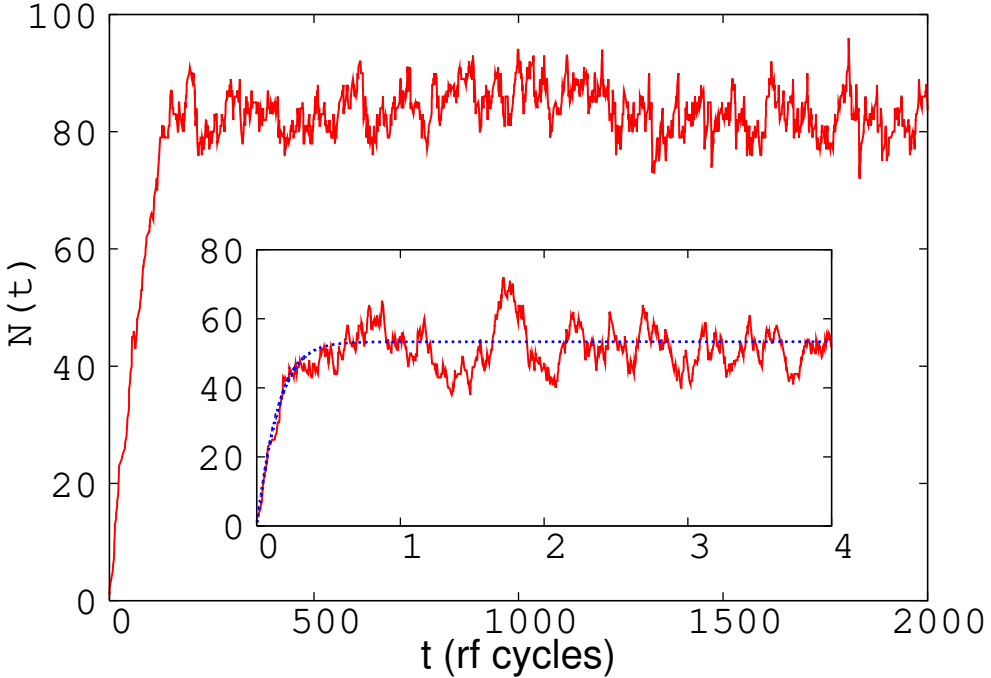


FIG. 1: (Color online) Number of particles  $N(t)$  in a 3D Paul trap as a function of  $t$  (in rf cycles), loaded with loading rate  $\lambda = 1$  particle / rf cycle inside of a spherical volume of radius  $R = 3$  centered at the origin of the trap. Particles are absorbed at a critical distance  $R_c = 15$ . Trap control parameters are  $q = 0.2$ ,  $a = q^2/2$ . Inset: Test of the loading equation (2) for a loading rate  $\lambda = 300$  particles / rf cycle. Red solid line: Number of particles  $N(t)$  obtained via numerical simulation of the loading process. Blue dotted line: Prediction according to (4).

is accurately approximated by completely neglecting the trap potentials and treating the particles' dynamics as a Coulomb explosion [15]. In this case, in dimensionless variables, the temporal evolution of the number of particles,  $\tilde{N}(t)$ , inside of the loading region of radius  $R$  is described by the differential equation [16]

$$\frac{d\tilde{N}(t)}{dt} = \lambda - \left( \frac{\tilde{N}(t)}{R} \right)^{3/2}. \quad (2)$$

In the stationary state,  $d\tilde{N}(t)/dt = 0$  and we obtain from (2)

$$\tilde{N}_s(\lambda) = R \lambda^{2/3}. \quad (3)$$

Because of continuity, the steady-state number of particles in the trap,  $N_s(\lambda)$ , is proportional to the number of particles in the loading region,  $\tilde{N}_s(\lambda)$ . Therefore, the  $\lambda^{2/3}$  dependence of

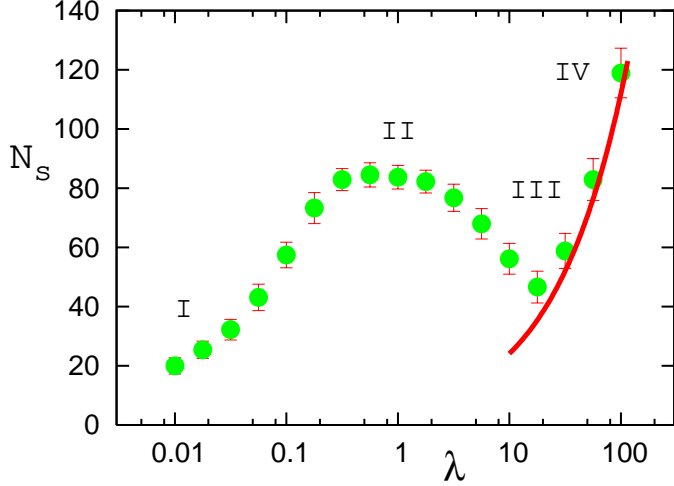


FIG. 2: (Color online) Nonmonotonic loading curve  $N_s(\lambda)$  for a 3D Paul trap with  $q = 0.2$ ,  $a = q^2/2$ ,  $R = 3$ , and  $R_c = 15$ . Solid green dots: Results of 3D molecular dynamics loading simulations. The red bars indicate the amplitudes of the  $N(t)$  fluctuations in the saturated state. For the first two dots the  $N(t)$  fluctuations are smaller than the plot symbols. The four distinct regions of the loading curve are labeled I to IV. The red solid line is the curve  $N_s(\lambda) = 5.2 \times \lambda^{2/3}$ , which confirms the  $\sim \lambda^{2/3}$  behavior of 3D Paul traps in Region IV.

$\tilde{N}_s(\lambda)$  is reflected in Fig. 2 (solid red line). Because there are more particles in the trap than there are in the loading zone, the pre-factor 5.2 of  $N_s(\lambda)$ , stated in the caption of Fig. 2, is larger than the pre-factor  $R = 3$  of  $\tilde{N}_s(\lambda)$ .

The solution of (2) can be stated implicitly in closed form:

$$t = -\frac{2R}{3\lambda^{1/3}} \left\{ \ln(\alpha - \tilde{N}^{1/2}) - \frac{1}{2} \ln(\tilde{N} + \alpha\tilde{N}^{1/2} + \alpha^2) \right. \\ \left. + \sqrt{3} \arctan \left( \frac{2\tilde{N}^{1/2} + \alpha}{\alpha\sqrt{3}} \right) - \sqrt{3} \arctan \left( \frac{1}{\sqrt{3}} \right) \right\}, \quad (4)$$

where  $\alpha = R^{1/2}\lambda^{1/3}$ . Since the trap potentials are not important in Region IV, the results (2) – (4) apply universally to all rf traps, e.g., 3D or linear Paul traps.

In order to test (4), we chose  $R = R_c = 3$  and a large loading rate of  $\lambda = 300$  particles / rf cycle. The result of the corresponding molecular dynamics simulation of  $N(t)$  is shown as the solid, fluctuating red line in the inset of Fig. 1. The blue, dotted line in the inset of Fig. 1 is the prediction according to (4). Both agree perfectly within the expected fluctuations of  $N(t)$ , which are due to the Poissonian loading process.

While for large  $\lambda$  the trap potentials are not important, they become progressively more important when  $\lambda$  is lowered. In this case, for low enough  $\lambda$ , particles created close to the edge of the loading zone,  $r \sim R$ , no longer have enough energy to overcome the trap potentials at  $R_c$  and are reflected back into the interior of the trap. In this  $\lambda$  region, where back-reflection occurs, fewer particles escape and  $N_s(\lambda)$  increases for decreasing  $\lambda$  up to a maximum in Region II, effectively creating a dip in Region III (see Fig. 2). However, the reflected particles will not stay in the trap forever. Due to rf heating [10], and given enough time (small loading rates), these particles will heat out of the trap, eventually lowering the number  $N_s(\lambda)$  of stationary-state particles in the trap below the bottom of the valley (Region III in Fig. 2), thus explaining both the formation of the maximum in  $N_s(\lambda)$  (Region II in Fig. 2) and the eventual decline of  $N_s(\lambda)$  in the direction of ever diminishing loading rates (Region I in Fig. 2). Since rf heating is a universal feature of all rf charged-particle traps, the qualitative shape of  $N_s(\lambda)$  is expected to be universal for all rf traps.

To check the universality of the non-monotonic behavior, we also simulated a linear Paul trap [17] whose equations of motion, in the notation and units of (1), are given by

$$\begin{pmatrix} \ddot{x}_i + [a - 2q \sin(2t)]x_i - Bx_i \\ \ddot{y}_i - [a - 2q \sin(2t)]y_i - By_i \\ \ddot{z}_i + 2Bz_i \end{pmatrix} = \sum_{\substack{j=1 \\ j \neq i}}^{N_k} \frac{\vec{r}_i - \vec{r}_j}{|\vec{r}_i - \vec{r}_j|^3}, \quad (5)$$

where  $B$  is a positive constant. As the loading region we still take the spherical region with radius  $R$  centered at  $\vec{r} = 0$ . However, because of the approximate translational symmetry of the trap in the  $z$  direction, we define an absorbing cylinder around the  $z$  axis of radius  $R_c$ . Thus, particles are allowed to escape in  $r$  direction, but not in  $z$  direction. This is justified, since there is no rf component in  $z$  direction, which implies that the  $r$  direction heats much faster than the  $z$  direction and particle escape, therefore, is much faster in  $r$  than in  $z$  direction. We simulate the loading process of the linear Paul trap (5) in analogy to the 3D Paul trap (1) as discussed above with a spherical MOT loading zone of radius  $R$  located at the geometric center of the linear trap. This time, however, we use the equations of motion (5) between creation times. For  $R = 3$ ,  $R_c = 30$ ,  $q = 0.3$ ,  $a = 0$ , and  $B = 0.042$  (chosen to model the trap in [11]), we obtain the linear Paul trap saturation curve  $N_s(\lambda)$  shown in Fig. 3. We clearly see the four different regions of  $N_s(\lambda)$ , providing corroborating evidence for the universal nature of the shape of  $N_s(\lambda)$  for all types of rf traps.

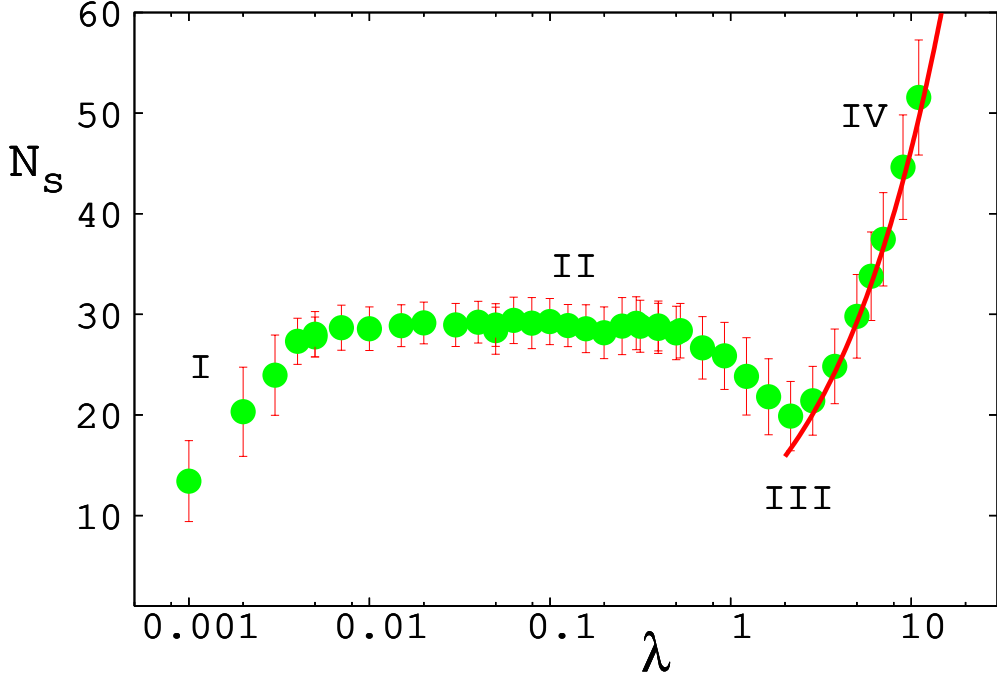


FIG. 3: (Color online) Nonmonotonic loading curve  $N_s(\lambda)$  for a linear Paul trap with  $q = 0.3$ ,  $a = 0$ ,  $B = 0.042$ ,  $R = 3$ , and  $R_c = 30$ . Solid green dots: Results of 3D molecular dynamics loading simulations. The red bars indicate the amplitudes of the  $N(t)$  fluctuations in the saturated state. The four universal regions I, ..., IV are clearly present. The red solid line is the curve  $N_s(\lambda) = 10.0 \times \lambda^{2/3}$ , which, in addition to 3D Paul traps (see Fig. 2), confirms the  $\sim \lambda^{2/3}$  behavior for linear Paul traps in Region IV.

While the non-monotonic behavior for 3D and linear Paul traps, e.g., is the same (compare Figs. 2 and 3), details are clearly different. The dip in Fig. 2, e.g., occurs at much larger  $\lambda$  than the dip in Fig. 3. This is a consequence of the absence of rf heating in the  $z$  direction of a linear trap, which leads to much reduced overall rf heating power, and thus a shift of the dip to lower  $\lambda$ .

The ultimate test of the correctness of the predictions is an experiment. We used a MOT-loaded ion-neutral hybrid trap [11] to test our predictions. Figure 4 shows the result of our experiments. All four predicted dynamical regimes are present and the shape of the experimental  $N_s(\lambda)$  curve is seen to be qualitatively the same as predicted by the model simulations and our qualitative analysis of the physical mechanisms that determine the steady-state population in rf traps. From the experimental data we obtain  $\epsilon = 0.745 \pm 0.098$  for the exponent  $\epsilon$  in  $N_s(\lambda) \sim \lambda^\epsilon$ , which is consistent with the predicted value  $\epsilon = 2/3$  in

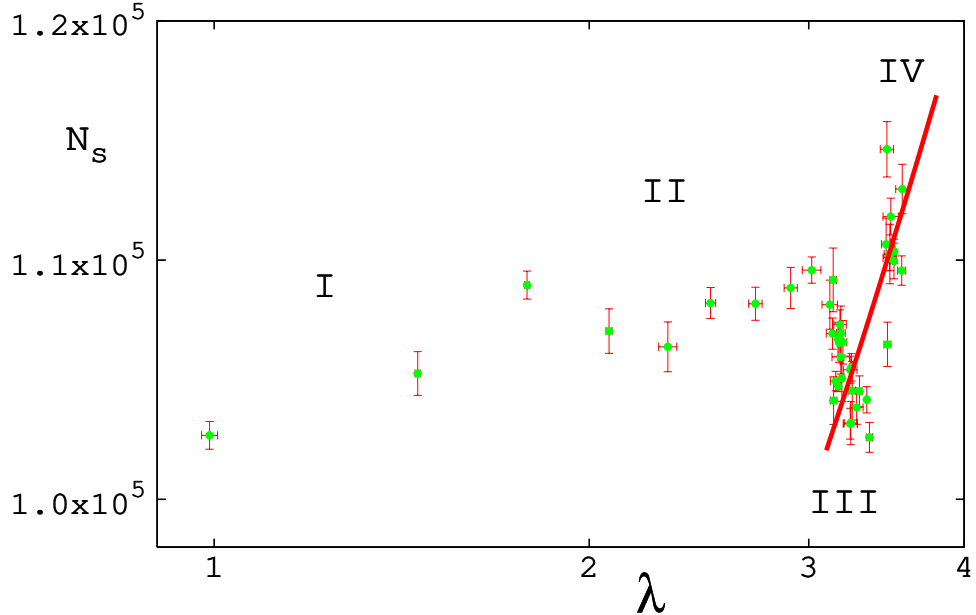


FIG. 4: (Color online) Experimental loading curve for the hybrid trap [11], operated with  $q = 0.26$ . All four predicted dynamical regimes are present. The red solid line is the curve  $N_s = 48000\lambda^{2/3}$ . The error bars represent the statistical errors associated with multiple data runs.

Region IV (red solid line in Fig. 4). We note that, corroborating the universality claim, the qualitative shape of the nonlinear behavior of  $N_s(\lambda)$  was observed in all of our simulations and experiments, independent of rf amplitudes, rf frequencies, and MOT sizes.

In the interest of reasonable simulation times, our numerical linear trap is a scaled-down version of our experimental trap, which results in saturated particle numbers that are in the hundreds, which is computationally manageable, rather than in the hundred thousands, which is far beyond our computational resources. However, within our computational limits, we checked that the qualitative shape of  $N_s(\lambda)$  is independent of particle number. Thus, our numerical simulations, while not exact one-to-one models of our actual experimental trap, provided both motivation for our laboratory experiments and another aspect of universality, i.e. independence of trap size and the accompanying order of magnitude of the number of stored particles in the steady state.

To strengthen the universality claim and the robustness of our predictions, we performed numerous additional simulations intended to demonstrate that the qualitative shape of the saturation curve, characterized by its four dynamical regimes, is insensitive to the details of our simulations. In particular, we ran additional simulations with (a)  $R$  ranging from 0.5

to 3, (b) replacing the Poissonian distribution of loading times with a uniform distribution, (c) replacing the uniform spatial distribution with a Gaussian distribution, (d) varying  $R_c$  between 15 and 30 (which also changes the absolute particle number in the saturated state up to a factor of 3), and (e) replacing the spherical absorbing boundary with radius  $R_c$  with a box of side length  $R_c$ . All five numerical tests confirmed the qualitative shape of  $N_s(\lambda)$  as shown in Figs. 2 and 3.

Most of our current simulations are conducted with a spherical loading region, since it closely models the MOT loading region of our experiments. However, since the same physical mechanisms are at work that result in the regimes I to IV, other loading geometries, e.g. elliptical or cylindrical (e.g., caused by the beam of an electron gun), are expected to result in the same universal shape of  $N_s(\lambda)$ . For elliptical loading regions we checked explicitly that this is indeed the case.

In this paper we presented evidence for the universality of the non-monotonic shape of the saturated ion number  $N_s(\lambda)$  of rf traps as a function of loading rate  $\lambda$ . Four dynamical regions are predicted. In Region I  $N_s(\lambda)$  increases monotonically with  $\lambda$ , reaching a maximum (Region II) at intermediate loading rates  $\lambda$ , followed by a valley (Region III), and an ultimate  $\sim \lambda^{2/3}$  increase of  $N_s(\lambda)$  for very large loading rates. We argue that the four regions are expected on the basis of physical reasons and are caused by the interplay between trap potentials, space-charge effects, and rf heating. The validity of the predictions, in particular their universality, are corroborated with the help of microscopic molecular-dynamics simulations of a 3D Paul trap and a linear Paul trap, which both show the predicted qualitative shape of  $N_s(\lambda)$ . The theoretical predictions are confirmed experimentally with the help of  $\text{Na}^+$  ions in a MOT-loaded linear Paul trap.

While loading an rf trap is important, so is the *decay* of the particle population in an rf trap, which starts as soon as the source of the charged particles is switched off. Particle decay is a natural consequence of rf heating, since the stored particles will be “heated out of the trap”. In analogy to the unexpectedly rich phenomenology of the loading stage of rf traps, explored in this paper, we expect similarly rich non-exponential dynamical behavior in the decay stage of rf traps [11]. We are confident that, in analogy to the loading stage, a more detailed investigation of the decay stage will uncover a multitude of new dynamical phenomena whose manifestations and physical underpinnings are important ingredients for the proper interpretation of experimental data based on the decay of particle populations

in rf traps.

Financial support by NSF grant number 1307874 is gratefully acknowledged.

---

- [1] W. Paul, *Rev. Mod. Phys.* **62**, 531 (1990).
- [2] H. Dehmelt and N. Yu, *Proc. Natl. Acad. Sci. U.S.A.* **94**, 10031 (1997).
- [3] C. Champenois, M. Knoop, M. Herbane, M. Houssin, T. Kaing, M. Vedel, and F. Vedel, *Eur. Phys. J. D* **15**, 105 (2001).
- [4] R. Alheit, Th. Gudjons, S. Kleineidam, and G. Werth, *Rapid Comm. Mass Spectr.* **10**, 583 (1996).
- [5] C. A. Schrama, E. Peik, W. W. Smith, and H. Walther, *Opt. Comm.* **101**, 32 (1993).
- [6] J. C. Bergquist, W. M. Itano, and D. J. Wineland, *Phys. Rev. A* **36**, 428 (1987).
- [7] J. C. Bergquist, S. R. Jefferts, and D. J. Wineland, *Phys. Today* **54**(3), 37 (2001).
- [8] J. I. Cirac and P. Zoller, *Phys. Rev. Lett.* **74**, 4091 (1995).
- [9] S. Gulde, D. Rotter, P. Barton, F. Schmidt-Kaler, R. Blatt, and W. Hogervorst, *Appl. Phys. B* **73**, 861 (2001).
- [10] R. Blümel, J. M. Chen, E. Peik, W. Quint, W. Schleich, Y. R. Shen, and H. Walther, *Nature* **334**, 309 (1988).
- [11] D. S. Goodman, J. E. Wells, J. M. Kwolek, R. Blümel, F. A. Narducci, and W. W. Smith, *Phys. Rev. A* **91**, 012709 (2015).
- [12] S. Lee, K. Ravi, and S. A. Rangwala, *Phys. Rev. A* **87**, 052701 (2013).
- [13] D. S. Goodman, I. Sivarajah, J. E. Wells, F. A. Narducci, and W. W. Smith, *Phys. Rev. A* **86**, 033408 (2012).
- [14] J. D. Tarnas, Y. S. Nam, and R. Blümel, *Phys. Rev. A* **88**, 041401(R) (2013).
- [15] Z. Vager, R. Naaman, and E. P. Kanter, *Science* **244**, 426 (1989).
- [16] R. Blümel, J. E. Wells, D. S. Goodman, J. M. Kwolek, and W. W. Smith, in preparation.
- [17] M. G. Raizen, J. M. Gilligan, J. C. Bergquist, W. M. Itano, and D. J. Wineland, *Phys. Rev. A* **45**, 6493 (1992).